Journal of Materials Chemistry C

RSC Publishing

PAPER

Anomalous transmittance of polystyrene–ceria nanocomposites at high particle loadings†

Cite this: *J. Mater. Chem. C*, 2013, **1**, 290

Onur Parlak and Mustafa M. Demir*

Received 31st August 2012
Accepted 16th October 2012

DOI: 10.1039/c2tc00084a

www.rsc.org/MaterialsC

Optical nanocomposites based on transparent polymers and nanosized pigment particles have usually been produced at low particle concentrations due to the undesirable optical scattering of the pigment particles. However, the contribution of the particles to many physical properties is realized at high concentrations. In this study, nanocomposites were prepared with transparent polystyrene (PS) and organophilic CeO_2 nanoparticles using various compositions in which the particle content was up to 95 wt%. The particles, capped by 3-methacryloxypropyltrimethoxysilane (MPS), were dispersed into PS and the transmittance of the spin-coated composite films was examined over the UV-visible region. When the particle concentration was <20 wt%, the transmittance of the films showed a first-order exponential decay as the Rayleigh scattering theory proposes. However, a positive deviation was observed from the decay function for higher particle contents. The improvement in transmittance may be a consequence of interference in the multiple scattering of light by the quasi-ordered internal microstructure that gradually develops as the particle concentration increases.

1 Introduction

Transparent commodity polymers such as polystyrene (PS) and poly(methyl methacrylate) represent a lower-cost and lighter-weight alternative with better impact resistance than the widely used inorganic glass due to their comparable structural homogeneity and optical clarity.[1–4] At the same time, they are highly appealing for integration into emerging flexible electronics. Their significantly higher humidity repellency as compared to inorganic glass could facilitate improvements in optoelectronic devices. The blending of these polymers with nanosized inorganic pigment particles presents a practical and promising approach to producing optical materials with various functionalities such as absorption/emission at the desired region of the optical spectrum and high/low refractive indices for tunable focusing. Potential applications could be in displays, waveguides, and solar cells' frequency converters, as well as nonlinear optical applications such as logic elements in nanoscale optoelectronic circuitry.[5–9] The main disadvantage of polymeric nanocomposites is visible light scattering due to the particle domains in the transparent polymeric medium. The sharp refractive indices increasing at the polymer–pigment particle interface cause optical scattering and the transmittance of the composites is remarkably reduced. The Rayleigh scattering theory can be applied to determine intensity loss due to scattering with the following expression:[10]

$$T = \exp\left[-\frac{3\phi r^3}{4\lambda^4}\left(\frac{n_p}{n_m} - 1\right)\right] s \qquad (1)$$

where T is the transmission, s is the optical path length (thickness of the film), r is the radius of the scattering element, ϕ is the volume fraction of the particles, λ is the wavelength of the incident light, and n_p and n_m are the refractive indices of the particles and the polymer matrix, respectively. It must be noted that the size of the scattering element is the strongest parameter. For example, when the size of the scattering element is doubled, transmission decreases by more than two orders of magnitude. The key point in the fabrication of transparent heterogeneous systems is to reduce the size of the scattering element to smaller than 100 nm. In polymer–particle nanocomposite systems, scattering elements are particle domains. A domain is composed of either an individual particle or a group of particles.[4] Depending on the size of the domain and the extent of the interaction of individual nanoparticles, a domain can be an aggregate, agglomerate, or cluster. All of these structures in fact are related to the level of particle dispersion in the polymer matrix. The formation of different domain structures is mainly governed by the volume fraction of the particles. In dilute composites where the amount of particles with respect to the polymer matrix (percentage) is low, the particles generally exhibit homogeneous dispersion with a small domain size. On the other hand, in dense composites, the particles have more

Department of Chemistry, Materials Science and Engineering Program, İzmir Institute of Technology, Gülbahçe Köyü, Urla, 35430 İzmir, Turkey. E-mail: mdemir@iyte.edu.tr; Fax: +90 232 750 75 09; Tel: +90 232 750 75 11

† Electronic supplementary information (ESI) available: DLS intensity and volume size distributions of surface-modified CeO_2 particles, XRD patterns of unmodified and MPS-modified CeO_2 nanoparticles, TGA of modified and unmodified CeO_2 particles, and FTIR of MPS molecules and neat and MPS-modified ceria. See DOI: 10.1039/c2tc00084a

probability of touching each other and a strong tendency to form large particle domains. Surface modification of nanoparticles may render the particles homogeneously dispersed in the polymer matrix. However, the formation of large particle domains inevitably occurs due to the interparticle depletion attraction as the particle content increases, even if the particles are effectively surface-modified. Therefore, the size of particle domains (scattering elements) is not an independent parameter; rather, it strongly depends on the volume fraction of particles. In dense composites, strong optical scattering takes place not only because of the increased particle concentration but also due to the increase in the size of particle domains. There is a tradeoff between transmission and particle content. This is because the majority of works on the fabrication of transparent nanocomposites have been devoted to dilute composites. However, the contribution of particles at high particle concentrations has been realized toward many physical properties, such as the refractive index,[11,12] conductivity,[13–15] elastic modulus,[16–18] or scratch resistance.[19,20] The maintenance of transparency is a major challenge while certain physical properties are improved at high levels of particle contents. Recently, Tsuzuki reported the possibility of fabricating highly transparent nanocomposite films with a controlled refractive index based on ZnO and caprylic capric triglyceride 60 wt% (~8 vol%).[21] The author showed that the refractive index of the resulting composite was modified and controlled by the particle concentration; it increased linearly as the particle content increases. However, the transmission of the composites did not show a systematic decrease, but rather saturated to a near-constant value at high particle loadings. It was claimed that the interference in the multiple scattering of the particle domains may lead to high transmission values.

There are important lessons that scientists can take from nature about the design and fabrication of novel materials.[22] The cornea, the front covering of eye, is a good example of this, particularly in the context of transparent polymer nanocomposites. It is a composite material made up of long collagen nanofibers embedded into a proteoglycan matrix. The fibers constitute a very high proportion (about 82%) of the dry weight of the cornea; in other words, the cornea is a dense composite.[23] The refractive index of the collagen fibril is different than that of the proteoglycan matrix. One may expect that a strong scattering takes place in the cornea and makes the material opaque. However, the cornea has excellently high transparency, the origin of which is still not clearly understood. The physical basis of the cornea is considered to be the arrangement of the collagen fibrils in the matrix such that the fibrils do not scatter independently of one another.[23] The scattering is suppressed as a result of the mutual interference of the scattered light. Inspired by the transparency of the cornea, in this work, we prepared dense nanocomposites by blending inorganic pigment particles (ceria) and a transparent commodity polymer (polystyrene). Ceria is a wide band gap semiconductor. It has many applications in various fields, such as UV absorbance,[24] catalytic converters in automobiles,[25] ion conducting in solid oxide fuel cells,[26] oxygen storage,[27] and gas sensing.[28] In addition, it has a high refractive index, above 2.0 at 550 nm.[29] Polystyrene (PS), meanwhile, is one of the most widely used plastics. It has aromatic benzene groups on a polymer backbone, and so PS has a relatively higher refractive index (1.59 at 633 nm) compared to many organic materials.[30] It is a colorless, transparent, and rigid plastic whose transmittance is over 90% at normal incidence.[31] The association of ceria and PS offers a convenient model system for the study of transmittance of the resulting composite material at different compositions. The difficulty in preparing homogeneous composites at high particle concentrations is the need for a large amount of nanosized organophilic particles that exhibit uniform and aggregate-free dispersion in the polymer matrix. We demonstrated the preparation of gram-scale CeO_2 nanosized particles capped by 3-methacryloxypropyltrimethoxysilane (MPS). The choice of this surfactant was based on the results of our previous work. We tested the dispersibility of CeO_2 nanoparticles capped with various surfactants such as 3-(mercaptopropyl) trimethoxysilane, hexadecyltrimethyl ammonium bromide, 3-mercapto propionic acid, and thioglycolic acid.[32] The particles capped with 3-methacryloxypropyltrimethoxysilane showed individual particle dispersion in an organic medium while the ones capped with other surfactants exhibited larger aggregates. The MPS capped particles were homogeneously dispersed into a PS matrix by solution blending in tetrahydrofuran (THF) with a wide range of particle concentrations of up to 95.0 wt%. The transmittance of the composite films was found to be a function of particle concentration. It showed a first-order exponential decay with particle content for dilute composites, as expected from eqn (1). On the other hand, higher transmission was obtained compared to the decay function in dense composites. At high particle concentrations, the particle domains are forced into a quasi-ordered structure. The increase in transmission may be a consequence of the interaction of visible light with the ordered microstructure that is inevitably developed as the particle concentrations increase.

2 Experimental section

2.1 Materials

Cerium nitrate hexahydrate (99.9%) was obtained from Fluka. Urea (ACS reagent, 99.0%), MPS (99.0%), THF (99.9%), and PS were purchased from Sigma-Aldrich and were used without further purification. Dimethyl formamide (DMF) (99.0%) was obtained from Riedel de Haën and was used as received.

2.2 Nanoparticle synthesis and surface modification

The one-pot synthesis and modification of CeO_2 nanoparticles was carried out by controlled precipitation. In the synthesis, nanoscale ceria particles were precipitated from a mixture of $Ce(NO_3)_3 \cdot 6H_2O$ and urea solutions of DMF. The standard for precipitation was as follows: equal volumes (12.5 mL) of 0.5 M $Ce(NO_3)_3 \cdot 6H_2O$ and 1.5 M urea solution were mixed at 120 °C, then refluxed under mild stirring for 1 h. In the modification, 0.5 mL of MPS in 5 mL of DMF was injected into the reaction medium after about 5 min under nitrogen atmosphere. The reaction of the medium was kept at 0–10 °C to prevent

homocondensation of the silane groups. The mixture was then further stirred at room temperature for 12 h to achieve a uniform surface coverage. The resulting suspension was isolated by centrifugation and rewashed several times to remove all residues. The product was then collected and dried in a vacuum at 50 °C for 8 h.

2.3 Preparation of PS–CeO_2 nanocomposite films

The surface-modified CeO_2 particles were dispersed into a PS solution of THF (20.0 wt% PS) at different concentrations and kept overnight in the dispersed state. After sonication for 30 min, composite films were prepared using a model WS 400B Spin Coater (Laurell Technologies Corp., North Wales, PA, USA) on quartz substrates. The films were annealed at 100 °C for 2 h.

2.4 Characterization

A VnmrJ 400 MHz broadband NMR spectrometer (Varian, Palo Alto, CA, USA) with a 5 mm probe was used to collect the spectra. They were continuously recorded and scans were averaged in blocks of 5 min up to 1 h of collecting time. X-ray diffractograms were obtained with a Philips X'pert Pro X-ray diffractometer using Cu Kα radiation ($\lambda = 1.5418$ Å). The size of the particles was determined using a Nano ZS dynamic light-scattering (DLS) instrument (Malvern Instruments, Worcestershire, UK). An atomic force microscope (AFM; Nanoscope IV, Digital Instruments-MMSPM, Tonawanda, NY, USA) was used to investigate the dispersion of the particles in the PS matrix. Transmission of the nanocomposites was measured with a Cary 50 UV-Vis Spectrometer (Varian). The resolution of the spectrophotometer was 1.5 nm and the photometric accuracy was ±0.01 in absorption. Transmission electron microscopy (TEM) was performed using a G^2 Spirit/Biotwin (FEI-Technai, Hillsboro, OR, USA) with a working voltage of 120 kV. FTIR measurements were carried out using a PE 100 FTIR spectrometer (PerkinElmer, Waltham, MA, USA). Film thicknesses were measured with a profilometer using a Dektak 150 (Veeco, Plainview, NY, USA).

3 Results and discussion

3.1 MPS-capped CeO_2 nanoparticles

Crystalline CeO_2 nanoparticles were obtained by the controlled precipitation of a mixture of $Ce(NO_3)\cdot 6H_2O$ and urea in DMF. Urea was decomposed into formaldehyde and ammonium hydroxide, thereby increasing the pH of the solution at which the precipitation takes place.[33] MPS molecules were added to the reaction medium as a surfactant. MPS has a silicon-centered group that can form chemical and physical bonds with a metal oxide surface, and it also has an organic group for the wetting of the particle surface by matrix chains. The precipitation of particles was carried out both in the absence and the presence of MPS to see the effect of surface modification. Fig. 1 shows the number size distribution of neat and *in situ* surface-capped CeO_2 particles after their isolation and redispersion in DMF (the volume and intensity distributions are given in Fig. S1†). While the neat particles have nearly micron-scale dimensions and a broad size distribution, the surface-capped particles exhibit a narrower size distribution with a mean diameter of 18 nm, and the entire population of the particle domain is smaller than 50 nm. Fig. 2 shows a representative overview TEM image of the

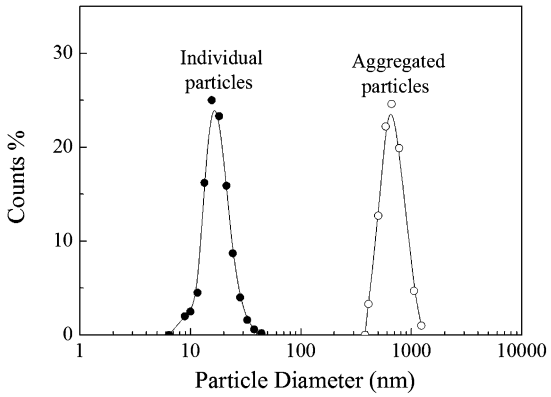

Fig. 1 DLS number size distribution of unmodified CeO_2 and MPS-modified CeO_2 particles at reaction medium after 1 h of reaction time.

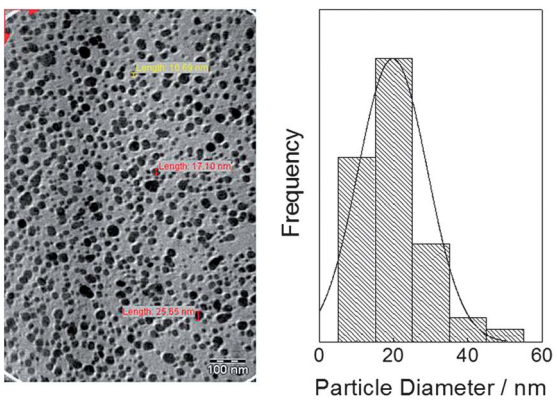

Fig. 2 TEM micrograph and particle size distribution of MPS-modified CeO_2 particles.

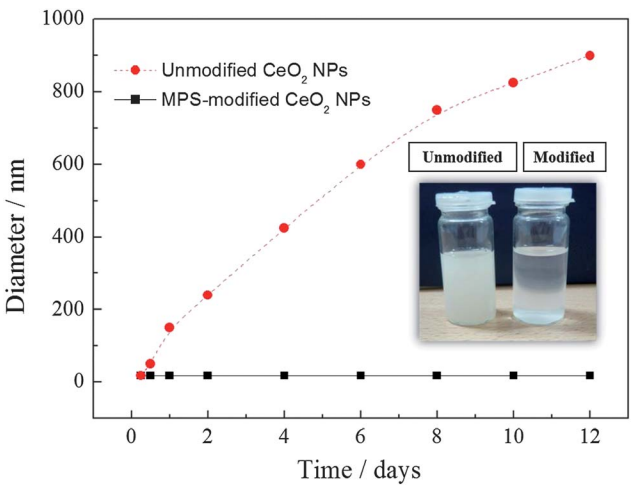

Fig. 3 The mean diameter of particles measured by DLS *in situ* for 12 h. Inset: photographic image of dispersions prepared with unmodified and modified particles.

CeO_2 nanoparticles. The crystals are spherical in geometry. The mean diameter of the size distribution is around 20 nm, comparable to the size measured by DLS. To gain further insight about the role of nanoparticles in the course of particle precipitation, the sizes of the formed particles were periodically measured *in situ* over the course of 12 days using DLS. Fig. 3 represents the mean diameter of the particles at different times of the reaction period under continuous stirring. The size of the particles prepared in the absence of MPS gradually increased from nanometer to micrometer scale. However, the diameter of the particles precipitated in the presence of MPS was around 18 nm, remaining almost unchanged for the entire time period. Two dispersions were prepared from the modified and unmodified CeO_2 particles. The dispersion prepared with MPS-capped particles was translucent (1 cm path length) even after 12 days of aging. The surface-capped particles are small enough and have a high dispersibility, and so optical scattering is avoided in the dispersion. On the other hand, the dispersion prepared with unmodified particles was completely opaque due to the rapid aggregation of the individual particles and the scattering of the aggregates. There are two possible ways of describing the particle growth in a reaction medium: Ostwald ripening and aggregation. The particles nucleate and they grow *via* a dissolution/precipitation process; large particles grow at the expense of smaller particles (Ostwald ripening).[34,35] They then rapidly combine to give a stable aggregate. The aggregates would further combine to give the next most stable aggregate, and so on. The occurrence of this mechanism many times in the absence of MPS causes a dramatic increase of particle dimension.[36] MPS molecules grafted to the surface of nuclei prevent the transfer of reactive species to and from the surface. Therefore, the growth of crystalline particles is strongly suppressed and aging does not affect the size of particles formed *in situ*. Note that the surface modification by MPS does not affect the crystalline nature of the CeO_2 particles (Fig. S2†).

Solution-state ^{1}H-NMR spectroscopy of the MPS-capped particle dispersion revealed that chemical bonds were formed between the MPS and particle surfaces. The particle surface is inevitably covered by surface hydroxyl groups.[37–39] Fourier transform infrared spectrometry of the particles showed a broad

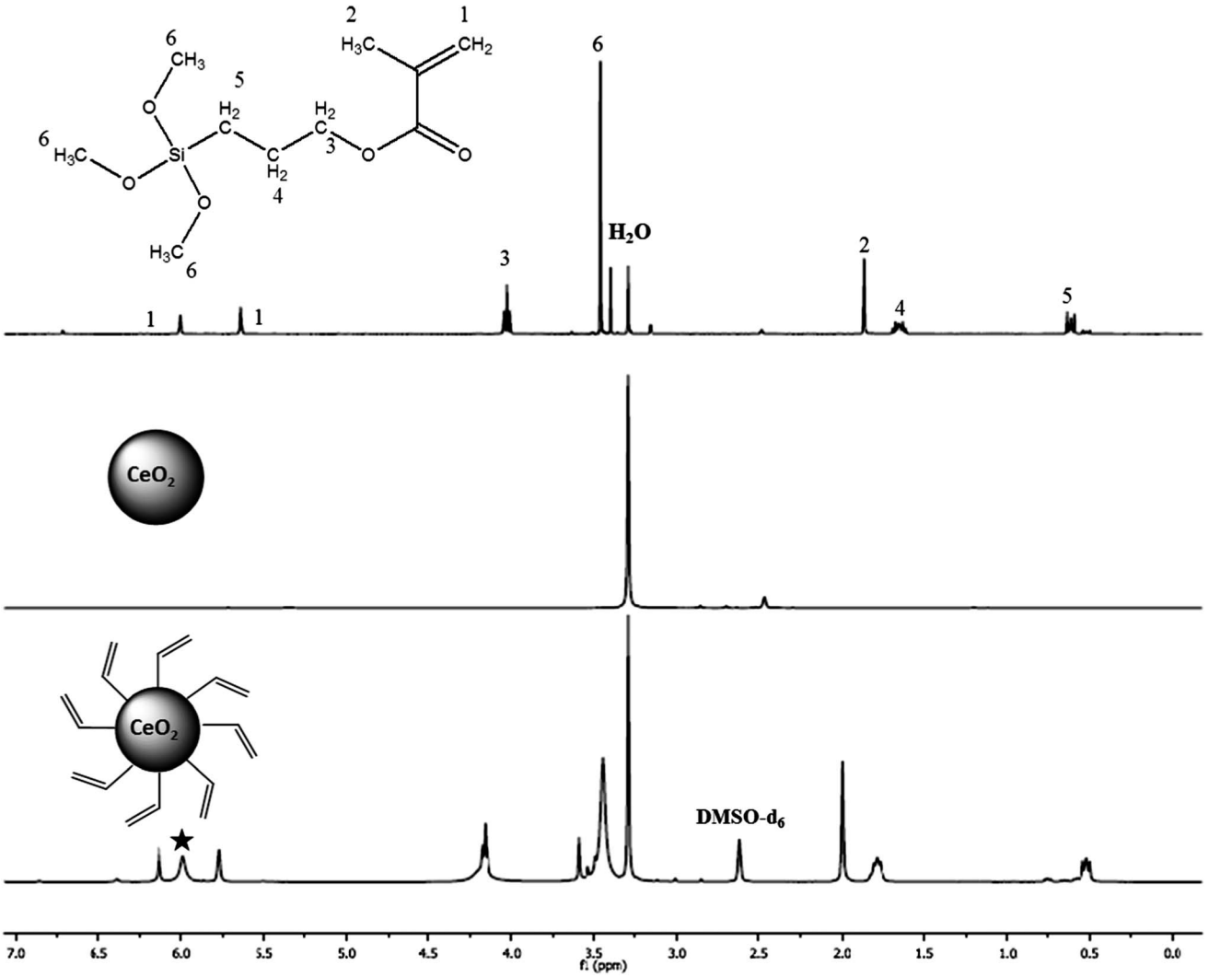

Fig. 4 ^{1}H-NMR spectra of (a) MPS itself, (b) unmodified CeO_2 particles, and (c) MPS-modified CeO_2 particles dispersed in DMSO-d_6.

vibrational signal centered around 3400 cm^{-1}, indicating the presence of surface hydroxyl groups (Fig. S4†). MPS grafts to the particle surface *via* condensation between the methoxide groups of silane and surface hydroxyl groups. Fig. 4 presents the ^{1}H-NMR spectra of MPS itself (curve a), unmodified CeO_2 particles (curve b), and MPS-modified CeO_2 nanoparticles (curve c). In curve a, the resonance signals at 6.3 and 5.6 ppm are assigned to the methylene protons (H1). The three resonance signals at 4.2, 1.7, and 0.5 ppm can be attributed to the α-CH_2, β-CH_2, and γ-CH_2 protons (signals H3, H4, and H5) of methacrylate, respectively. The signal at 1.8 ppm is assigned to the methyl protons near the vinyl group (peak H2); that at 3.5 ppm is caused by the methylene protons of trimethoxysilane (peak H6). For the spectrum of unmodified CeO_2 (curve b), there is no proton signal other than H_2O in d-DMSO.[40] Curve c shows the spectrum of MPS-modified CeO_2 nanoparticles. The characteristic signals of the MPS molecule are observed in this spectrum. There is no remarkable shift in the signals; however, a significant broadening was observed. When the protons are immobilized or absorbed at the surface of nanoparticles, the proton motion will become more restricted and the signals will become broader, or they will give a much weaker NMR-response or disappear.[41]

In the spectrum of the MPS-modified CeO_2 particles, along with the signals of MPS, a new signal in the spectrum, designated with an asterisk, appears at 6.0 ppm. There are two different grafting configurations of MPS molecules to the particle surface: perpendicular and parallel orientations. These are shown in panel a and panel b of Scheme 1, respectively.[42] The former configuration was described above; it is based on the condensation of surface hydroxyls and methoxide groups. Stable Si–O–C bonds form. In the latter configuration, along with the formation of Si–O–C bonds, hydrogen bonding may be induced between the carbonyl groups of MPS and surface hydroxyl groups. The new signal at 6.0 ppm in the NMR spectrum of MPS-modified CeO_2 nanoparticles can be attributed to the parallel configuration. The integration of the signals originating from parallel and perpendicular configurations suggests that neither configuration is dominant and that the grafting configurations occur evenly on the surface of CeO_2 particles. The graft density depends on the chemistry of substrate, thus deviating from estimates due to incomplete coverage or as a result of the formation of multilayers. The experimental values reported in the literature for the surface coverage of various oxides by MPS range from 2.8 to 7.5 μmol m^{-2}.[43] In our particular case, the grafting density was deduced from the mass loss due to the decomposition of the MPS molecules. The amount of MPS adsorbed onto the CeO_2 surface was measured by thermogravimetric analysis (TGA). The mass difference between unmodified and MPS modified CeO_2 particles upon heat treatment gave a clue about the amount of MPS adsorbed onto the particle surface. The difference was found to be 4.4 wt % (Fig. S3†). Since the size of the particles is known from both DLS and TEM, the grafting density can be roughly estimated assuming that there is a monolayer and uniform surface grafting. The surface coverage was estimated at 2.3 μmol m^{-2}, or about 50–60% of a completely filled monolayer. FTIR spectra of the particles confirm that there are still hydroxyl and chemical traces of the reactants, such as a vibration nitrate group at 1384 cm^{-1} (Fig. S4†).

3.2 Polystyrene–CeO_2 nanocomposites

MPS-capped particles were dispersed into PS–THF solution and composite films were prepared by both spin coating and solution casting. The transmittance of the resulting composites was measured on the spin-coated films at normal incidence over the UV-Vis region. Fig. 5 presents transmission spectra of the composite films. The PS–CeO_2 films are absorbing over the UV region because both ceria and the pendant benzene groups of the matrix chains absorb UV light. The absorption coefficient of ceria is orders of magnitude higher than that of PS,[44–46] and so the higher the particle content is, the higher the UV blockage is. On the other hand, the films are transparent over the visible region. In dilute composites where the particle concentration is <20 wt%, the percent transmission rapidly decreases with particle content. The decrease in transmission slows when the particle concentration increases to moderate levels (60 wt%). At higher concentrations, the spectra of the concentrated films cross the spectra of dilute composites through the longer wavelengths of the visible region. Surprisingly, the increase of particle content does not reduce transmission; it even causes it

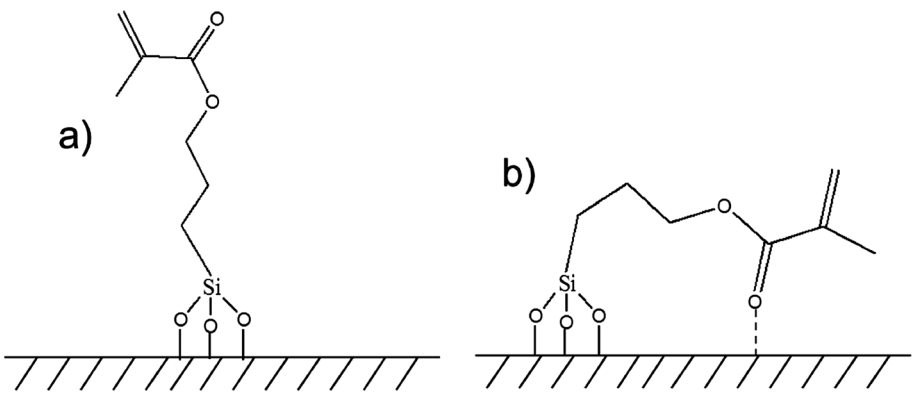

Scheme 1 Grafting configurations of MPS onto the surface of CeO_2 nanoparticles.

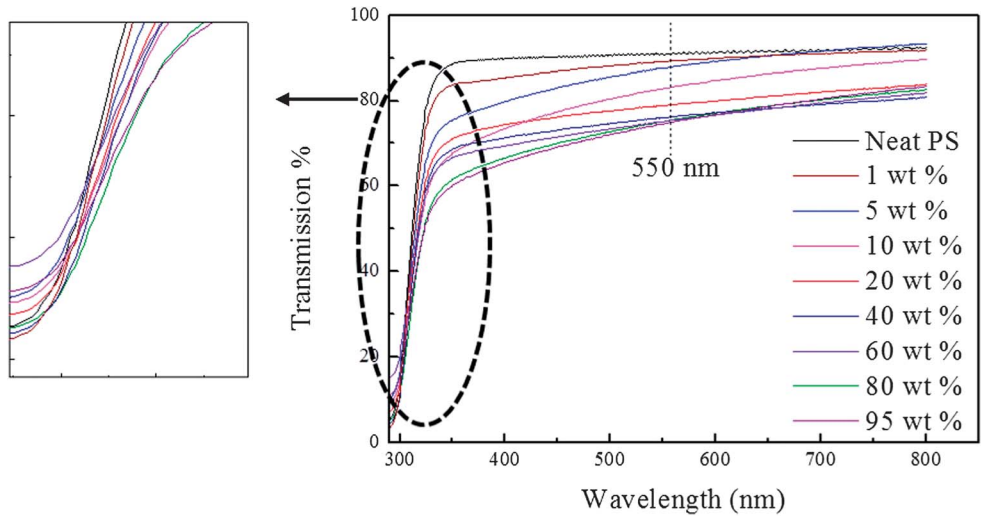

Fig. 5 Transmission spectra of the spin-coated PS composite films prepared with different amounts of MPS-modified particles. The thickness of the films was around 2.5 μm.

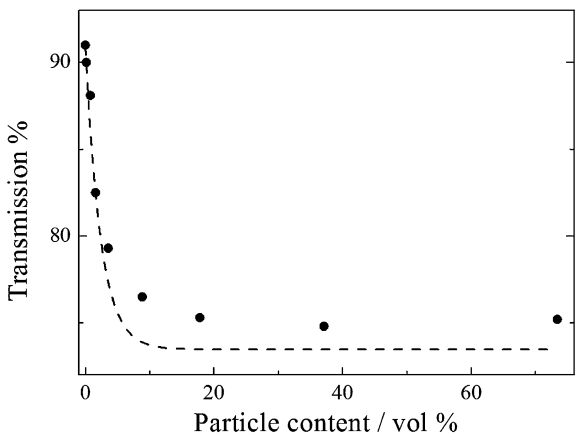

Fig. 6 Experimental transmission (data points) of the spin-coated composite films as a function of particle content at 550 nm. A first-order exponential decay function (dashed line) fit the data points. The data points were obtained from the transmission spectra of the films given in Fig. 5.

to increase. This discrepancy can be better seen when the transmission of the composites is plotted as a function of particle content at a particular wavelength. Fig. 6 presents percent transmission as a function of the volume fraction of particle content at a wavelength of 550 nm, where the human eye has the highest sensitivity. The transmission of the PS–CeO_2 composite films decays with the volume fraction of the particles. A first-order exponential decay function (shown as a dashed line) was fit to the data points using the Rayleigh scattering theory (eqn (1)). The transmission of neat PS is 92% at 550 nm. There is almost 8% surface reflection in our system at a normal incidence. The reflection takes place when light strikes the surface of a film. The light reflected from both air-to-film and film-to-substrate glass interfaces. At low particle concentrations, the data points agree with the decay function. In this regime, the results obey the Rayleigh theory. However, a deviation in favor of higher transmission takes place for the composites prepared with particle content higher than 20 wt% (4 vol%). The films systematically show 3–5% higher transmission than the decay function. This point is worth investigating because, to the best of our knowledge, an increase in transmission with particle content is not a frequently observed result in the literature.

The transmission of the composite films should be assessed from the basic principles of optics. In general, there are three types of mechanisms for the decrease of intensity of incident light: reflection (R), scattering (S), and absorption (A). Transmission is the remaining light after the occurrence of these three mechanisms during the interaction of light. The theoretical transmittance of a material can be estimated using eqn (2).

$$T = 1 - (R + S + A) \quad (2)$$

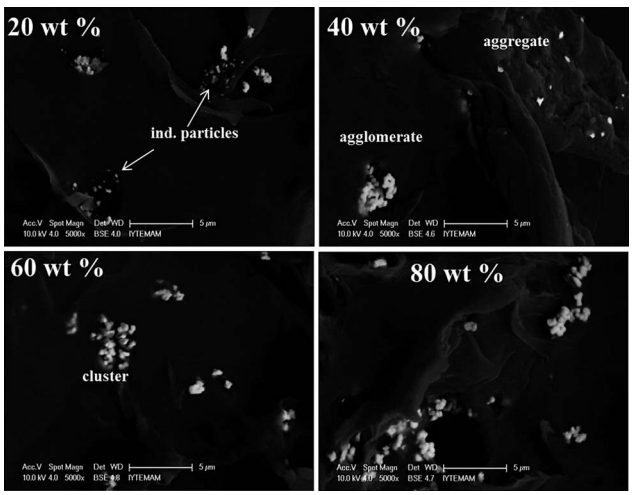

Fig. 7 SEM images of PS composites loaded with different amounts of MPS-modified particles (×5000).

The absorption term can be neglected for nonabsorbing films. The composite of PS and CeO_2 has negligible absorbance in the visible region. Surface reflection was also negligible at around 8% and is not a strong function of particle content. Therefore, the level of transmission is mainly determined by the extent of scattering. When scattering is reduced, transparency increases, and *vice versa*. The improvement of transmission at high particle concentrations was also compared with the sensitivity of the spectrophotometer employed in this measurement. The photometric sensitivity is ± 0.01 in absorption, which is multiple times smaller than the improvement in transmission. This result was reproducibly observed and therefore cannot have originated from the measurement techniques. Rather, it must be a consequence of the interaction of visible light with the internal structure developed at high particle concentrations.

The microstructure of a polymer–particle composite is mainly determined by the level and arrangement of particle dispersion in the polymer matrix.[47] A systematic study by microscopy was performed to determine the internal structure of the composites. Fig. 7 presents overview SEM images of the PS–CeO_2 cast films. The bright regions in the dark polymer matrix represent the particle domains due to the atomic number contrast between the polymer and CeO_2. Panel a of Fig. 7 presents an electromicrograph of the composite prepared with 20 wt% of ceria particles. The domains are composed of individual particles and small aggregates, both indicated with arrows. When the particle content was doubled, aggregates as well as large agglomerates were formed (panel b). The further increase of particle content to 60 wt% causes the formation of clusters along with agglomerates (panel c). At 80 wt%, even larger clusters and agglomerates appear in the bulk PS matrix (panel d). Using these electromicrographs, radial distribution functions, $g(r)$, were obtained for each composite from the negative of the images using the ImageJ program.[48] This function specifies the likelihood of finding two domains separated by a distance of r and it qualitatively describes the arrangement of particle domains in the structure. Fig. 8 presents the $g(r)$ of the PS–CeO_2 nanocomposites at different particle contents. Since two particle domains cannot approach closer than touching, $g(r)$ vanishes for separation distances smaller than the diameter of the particle domains. At low and even moderate levels of particle contents, there is no signal in the plot of $g(r)$, *i.e.* there are no distinguishing features in the arrangement of the particle domains. When the particle content increases to 60 wt%, a weak signal at around 1.5 μm appears. The intensity of the signal increases as the particle concentration increases. This result suggests that there is a high probability of finding a particle domain from a localized domain in the structure. Plots of the radial distribution function extend over even longer distances of 2–10 μm; in other words, the ordering is short-ranged.

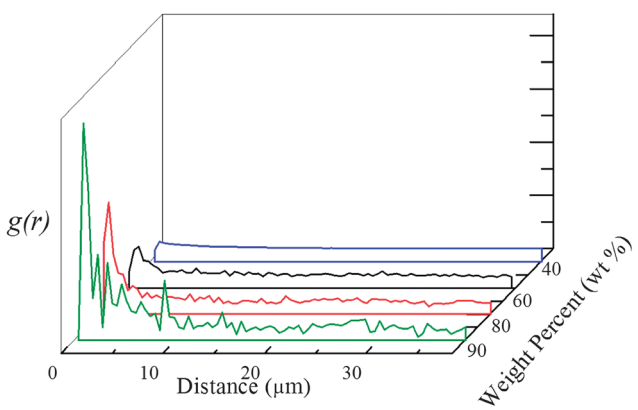

Fig. 8 Radial distribution functions, $g(r)$, obtained from data analysis of the SEM images given in Fig. 7. Image processing of electromicrographs shows a short-ranged ordering of particle domains at high particle contents.

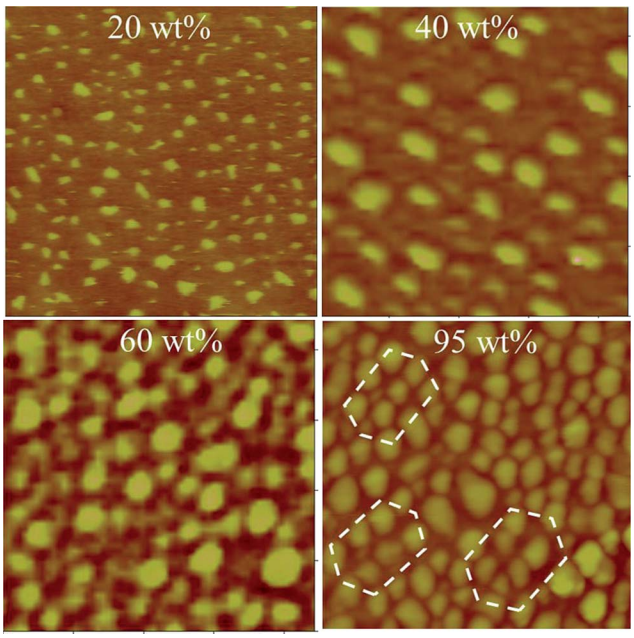

Fig. 9 Tapping-mode AFM images of PS composites loaded with different amounts of MPS-capped CeO_2 particles. The area of all images is 1.1 × 1.1 μm^2.

Table 1 The number density and mean diameter at different particle contents obtained by microscopy

Particle content [wt%]	Number particle domains	Mean diameter [nm]
20	153	33 ± 7
40	44	53 ± 10
60	92	61 ± 11
95	137	51 ± 14

High magnification images were obtained by AFM. Fig. 9 shows tapping-mode images where phase signals were acquired by scanning an area of 1.1 × 1.1 μm^2. Table 1 presents the average size and number density of the particle domains in the images. When the composites were prepared with 20 wt% of particles, the number density and average size of the domains were 153 and 33 ± 7 nm, respectively. The size of the domains is comparable with the size distribution obtained by DLS and TEM, indicating that the particle domains are either individual particles or small aggregates of individual particles. At 40 wt%, the number density is 44 and the size of particle domains is

increased to 53 ± 10. Further increase of particle content systematically increases the number density and the size of the particle domains. In AFM, a sharp tip slides across the surface of a specimen so that surface topography and phase contrast can be obtained from the outermost surface. However, AFM does not conclusively resolve individual particles in an aggregate and cannot correlate the number of individual particles in an aggregate.

When identical spherical objects are randomly added to a container, they are distributed randomly throughout the container. Increasing the number density of the spheres generally forms regular packing configurations. Similarly, when a droplet of dense polymer/particle suspension is cast on a substrate, the volume of the droplet shrinks upon solvent evaporation. This shrinkage generates a compressive force that draws the particles together. Once the domains touch each other, the receding interface forms menisci between them, and the resulting capillary forces collapse the particles into a cluster. This eventually dries the film and then consolidates and organizes the spherical particle domains into closely packed structures. AFM imaging of the composites prepared at higher levels of particle contents suggests the formation of hexagonal-type packing of ceria particle domains at 95 wt% (73 vol%). This concentration is in fact the limit of the theoretical compact packing of the spherical particles. Panel d of Fig. 9 shows representative examples of the hexagonal arrangement of the particle domains at different regions in the field of view of the image.

It is known in the literature that the interaction of light with an ordered material structure leads to an increase in transmission. Colloidal crystals are the extreme example of this. When uniform-sized particles are arranged in a perfect-ordered structure, the resulting material becomes perfectly transparent.[21,49] Considering the optical clarity of the colloidal crystal, the increase in transmission at high levels of CeO_2 particle contents in PS might be the result of the ordered microstructure of the polymer nanocomposites developed at high particle concentrations. In dilute composites, the number of scatterers (particle domains) is very low. The radiation is only scattered once by a localized scattering center, which is called *single scattering*. In this regime, the scattering elements are located at random positions and scattering occurs by a single scattering element independent of the others with a random efficiency. With moderate particle contents, a nanocomposite medium consists of a high number of scattering centers. The average distance between two scattering centers becomes much smaller than the dimensions (thickness) of the film. The light inside a strongly scattering nanocomposite medium is subjected to a large number of scattering events and *multiple scattering* arises. In dense composites, a quasi-ordered structure is developed and scattering elements are correlated in position. The randomness of the interaction tends to be averaged out. The *interference of multiply scattered waves* is added together to give a resultant wave intensity transmitted in the forward direction such that scattering is suppressed. As a consequence, the transmission of the composite films is improved. This mechanism may be active in the interaction of light with polymer–nanoparticle composites prepared at high particle contents.

4 Conclusion

In this work, we studied the transmittance of composites prepared from transparent PS and nanosized pigment CeO_2 particles at different compositions. MPS-capped CeO_2 nanoparticles with an average diameter of 18 nm were precipitated in a one-pot reaction using $Ce(NO_3)\cdot 6H_2O$ and urea. Gradual decomposition of urea catalyzes the precipitation of uniform ceria particles with a well-defined organophilic surface nature. MPS molecules as surfactants adsorb onto the surface of CeO_2. PS–CeO_2 nanoparticle composites were prepared at different compositions. For dilute composites where the particle content was <20 wt%, the particles were individually dispersed in the PS matrix. Increasing particle content enlarges the particle domains and increases their number density in the bulk PS. The radial distribution function of particle domains for each composite was obtained from scanning electron microscopy (SEM) images. The functions suggested a short-range order of particle domains for dense composites where the particle concentration was >40 wt%. At 95%, the particle domains were organized into a closely packed structure in a short-range order. The transmission of the spin-coated composite films was examined and compared with Rayleigh scattering. While perfect agreement between the experimental data points and the scattering model took place at low particle concentrations, the composite films prepared with high particle contents showed higher transmission. The contribution of the particle domains in optical scattering at high concentrations was found to be smaller compared to that at low particle concentrations. The origin of this effect is seen in the interaction of light with the quasi-ordered internal microstructure developed at high particle concentrations. The mutual interference of multiply scattered light by the ordered particle domains may be the cause of the improvement in transmission in the forward direction. This effect is realized when organophilic nanoparticles are dispersed in bulk polymer with a negligible amount of aggregation. These composite films can potentially be used in the design of optics and optoelectronics where both high loading of particles and transparency are simultaneously required.

Acknowledgements

The authors thank the Scientific and Technological Research Council of Turkey (TÜBİTAK) for support of research project TBAG-109T905, the specialist of the Materials Research Center for microscopy images, I. Özçelik for NMR measurements, and Prof. S. Özçelik of İzmir Institute of Technology for his critical reading of the manuscript.

References

1 Z. C. Cui, C. L. Lu, B. Yang, J. C. Shen, X. P. Su and H. Yang, *Polymer*, 2001, **42**, 10095–10100.
2 R. Okutsu, S. Ando and M. Ueda, *Chem. Mater.*, 2008, **20**, 4017–4023.
3 H. Dislich, *Angew. Chem., Int. Ed. Engl.*, 1979, **18**, 49–59.

4 M. M. Demir and G. Wegner, *Macromol. Mater. Eng.*, 2012, **297**, 838–863.
5 D. Koziej, F. Fischer, N. Kranzlin, W. R. Caseri and M. Niederberger, *ACS Appl. Mater. Interfaces*, 2009, **1**, 1097–1104.
6 R. Sreeja, J. John, P. M. Aneesh and M. K. Jayaraj, *Opt. Commun.*, 2010, **283**, 2908–2913.
7 B. Kulyk, B. Sahraoui, O. Krupka, V. Kapustianyk, V. Rudyk, E. Berdowska, S. Tkaczyk and I. Kityk, *J. Appl. Phys.*, 2009, **106**, 093102-1–093102-6.
8 A. H. Yuwono, B. H. Liu, J. M. Xue, J. Wang, H. I. Elim, W. Ji, Y. Li and T. J. White, *J. Mater. Chem.*, 2004, **14**, 2978–2987.
9 H. Ma, A. K. Y. Jen and L. R. Dalton, *Adv. Mater.*, 2002, **14**, 1339–1365.
10 B. M. Novak, *Adv. Mater.*, 1993, **5**, 422–433.
11 C. L. Lu, C. Guan, Y. F. Liu, Y. R. Cheng and B. Yang, *Chem. Mater.*, 2005, **17**, 2448–2454.
12 S. J. Ahmadi, Y. D. Huang and W. Li, *J. Mater. Sci.*, 2004, **39**, 1919–1925.
13 R. Gangopadhyay and A. De, *Chem. Mater.*, 2000, **12**, 608–622.
14 M. Moniruzzaman and K. I. Winey, *Macromolecules*, 2006, **39**, 5194–5205.
15 Z. Spitalsky, D. Tasis, K. Papagelis and C. Galiotis, *Prog. Polym. Sci.*, 2010, **35**, 357–401.
16 M. A. Osman, J. E. P. Rupp and U. W. Suter, *Polymer*, 2005, **46**, 1653–1660.
17 J. N. Coleman, U. Khan and Y. K. Gun'ko, *Adv. Mater.*, 2006, **18**, 689–706.
18 T. D. Fornes and D. R. Paul, *Polymer*, 2003, **44**, 4993–5013.
19 F. Tiarks, K. Landfester and M. Antonietti, *Langmuir*, 2001, **17**, 5775–5780.
20 F. Bauer, V. Sauerland, H. J. Glasel, H. Ernst, M. Findeisen, E. Hartmann, H. Langguth, B. Marquardt and R. Mehnert, *Macromol. Mater. Eng.*, 2002, **287**, 546–552.
21 T. Tsuzuki, *Macromol. Mater. Eng.*, 2008, **293**, 109–113.
22 D. A. Stone and L. T. J. Korley, *Macromolecules*, 2010, **43**, 9217–9226.
23 D. M. Maurice, *J. Physiol.*, 1957, **136**, 263–286.
24 O. Kepenekci, M. Emirdag-Eanes and M. M. Demir, *J. Nanosci. Nanotechnol.*, 2011, **11**, 3565–3577.
25 J. Kaspar, P. Fornasiero and M. Graziani, *Catal. Today*, 1999, **50**, 285–298.
26 E. P. Murray, T. Tsai and S. A. Barnett, *Nature*, 1999, **400**, 649–651.
27 H. C. Yao and Y. F. Y. Yao, *J. Catal.*, 1984, **86**, 254–265.
28 S. Gupta, S. Kuchibhatla, M. H. Engelhard, V. Shutthanandan, P. Nachimuthu, W. Jiang, L. V. Saraf, S. Thevuthasan and S. Prasad, *Sens. Actuators, B*, 2009, **139**, 380–386.
29 K. N. Rao, L. Shivlingappa and S. Mohan, *Mater. Sci. Eng., B*, 2003, **98**, 38–44.
30 *Polymer Handbook*, ed. J. C. Seferis, New York, 1999.
31 O. Parlak and M. M. Demir, *ACS Appl. Mater. Interfaces*, 2011, **3**, 4306–4314.
32 O. Tunusoglu, R. Munoz-Espi, U. Akbey and M. M. Demir, *Colloids Surf., A*, 2012, **395**, 10–17.
33 R. K. Jha, R. Pasricha and V. Ravi, *Ceram. Int.*, 2005, **31**, 495–497.
34 L. Meli and P. F. Green, *ACS Nano*, 2008, **2**, 1305–1312.
35 X. L. Jia, J. Listak, V. Witherspoon, E. E. Kalu, X. P. Yang and M. R. Bockstaller, *Langmuir*, 2010, **26**, 12190–12197.
36 L. Spanhel and M. A. Anderson, *J. Am. Chem. Soc.*, 1991, **113**, 2826–2833.
37 M. M. Demir, M. Memesa, P. Castignolles and G. Wegner, *Macromol. Rapid Commun.*, 2006, **27**, 763–770.
38 M. M. Demir, P. Castignolles, U. Akbey and G. Wegner, *Macromolecules*, 2007, **40**, 4190–4198.
39 M. A. Henderson, *Surf. Sci. Rep.*, 2002, **46**, 5–308.
40 H. E. Gottlieb, V. Kotlyar and A. Nudelman, *J. Org. Chem.*, 1997, **62**, 7512–7515.
41 O. Kohlmann, W. E. Steinmetz, X. A. Mao, W. P. Wuelfing, A. C. Templeton, R. W. Murray and C. S. Johnson, *J. Phys. Chem. B*, 2001, **105**, 8801–8809.
42 W. Posthumus, P. Magusin, J. C. M. Brokken-Zijp, A. H. A. Tinnemans and R. van der Linde, *J. Colloid Interface Sci.*, 2004, **269**, 109–116.
43 J. D. Miller and H. Ishida, *Surf. Sci.*, 1984, **148**, 601–622.
44 F. Wooten, *Optical Properties of Solids*, New York, USA, 1981.
45 C. G. Granqvist, *Handbook of Inorganic Electrochromic Materials*, Elsevier, Amsterdam, The Netherlands, 1995.
46 T. Inagaki, E. T. Arakawa, R. N. Hamm and M. W. Williams, *Phys. Rev. B: Solid State*, 1977, **15**, 3243–3253.
47 A. C. Balazs, T. Emrick and T. P. Russell, *Science*, 2006, **314**, 1107–1110.
48 Public domain software to be downloaded from http://rsb.info. nih.gov/ij, National Institutes of Health.
49 R. Buonsanti, A. Llordes, S. Aloni, B. A. Helms and D. J. Milliron, *Nano Lett.*, 2011, **11**, 4706–4710.

